Direct photon calculations in heavy-ion collisions at $\sqrt{s_{\rm NN}} = 62.4 - 200$ AGeV in a (3+1) dimensional hybrid approach

Bjørn Bäuchle[1,2,*] and Marcus Bleicher[1,2]

[1] *Frankfurt Institute for Advanced Studies, Frankfurt am Main, Germany*
[2] *Institut für Theoretische Physik, Goethe-Universität, Frankfurt am Main, Germany*

Direct photon spectra from central Au+Au- and Cu+Cu-collisions at $\sqrt{s_{\rm NN}} = 62.4, 130$ and 200 AGeV are calculated within the microscopic transport model UrQMD and a micro+macro hybrid model. In the latter approach, the high-density part of the transport evolution is replaced by an ideal 3+1-dimensional hydrodynamic calculation. We study the impact of viscosity and full local thermalization and compare the calculations to measurements obtained by the PHENIX collaboration. We find a reasonable agreement with the experimental data for calculations involving a Quark-Gluon-Plasma phase.

arXiv:1008.2332v1 [nucl-th] 13 Aug 2010

I. INTRODUCTION

Heavy-ion physics is widely used as a tool for the exploration of the phase diagram of strongly interacting matter. In the collision of heavy nuclei, the nucleons may be compressed and heated sufficiently to create a new state of matter that consists of partonic degrees of freedom, the Quark-Gluon-Plasma (QGP) [1, 2]. Indeed, proposed signatures for the QGP, like strong jet quenching and large elliptic flow have been found by experiments at the Relativistic Heavy Ion Collider (BNL-RHIC) [3–8].

Inferring knowledge about the central regions of a heavy-ion collision is very difficult, since even if a plasma is created, its lifetime and size are beyond the experimental reach for direct observation, so we are limited to the study of particles that are emitted from the reaction zone. Unfortunately, first principle calculations of QCD-processes are only possible if all involved scales are much larger than the QCD-scale $\Lambda_{\rm QCD} \approx 0.2$ GeV. However, in a heavy-ion collision, most particles have momenta comparable to $\Lambda_{\rm QCD}$. Therefore, more phenomenological approaches are necessary to explore the bulk of the matter.

While the abundance of hadronic particles that are produced in a heavy-ion collision are emitted at the end of the reaction and carry only indirect information from the early stages, electromagnetic probes allow for an undisturbed view into all stages of the reaction. Photons and leptons escape the reaction zone without rescattering due to their very small cross-section, but for the same reason, their abundancies are rather low, compared to hadronic species [9].

Three different electromagnetic particle species are currently being measured in heavy-ion experiments: single- and dielectrons, single- and dimuons and photons. Direct photons have the advantage that they are created in scatterings of the partonic or hadronic medium and are therefore directly coupled to the region of interaction. The leptons, however, are usually created in pairs, either in the (initial state) Drell Yan process or by the decay of hadrons. In addition, one of the leptons might be a neutrino, which escapes observation. Since this process is governed by the weak interaction, the decay usually happens outside the fireball. Single leptons are therefore used to reconstruct weakly decaying heavy quarks, while the invariant mass distribution of dileptons can be used to extract spectral functions of vector mesons.

Previous calculations of direct photons from transport theory include work with UrQMD by Dumitru *et al.* [10] and Bäuchle *et al.* [11] and with HSD by Bratkovskaya *et al.* [12]. Hydrodynamics has been used in many direct photon calculations, see e.g. [13–20].

The extraction of the yield of photons from the fireball (direct photons) is hindered by a huge background of photons from hadronic decays outside the fireball, which is dominated by the π^0- and η-decays. However, experimental techniques for the extraction of direct photon yields are well developed and allow to disentangle these late stage contributions from the scattering contribution. The experimental methods include a direct estimation of the background via invariant mass-analysis of the photons [21, 22], the analysis of interference patterns (using a Hanburry Brown-Twiss analysis) [23] and the extrapolation of the spectra of low-mass dileptons to the photon point [24].

In this paper, we apply a previously established model for direct photon emission from hadronic and partonic sources [11] and apply it to collision systems measured by the STAR and PHENIX collaborations at BNL-RHIC. In Section II, we briefly introduce the model and the parameters used for the present calculations, and in Section III we show the direct photon spectra obtained with our calculations as well as comparisons to the available data from the PHENIX collaboration [25, 26].

II. THE MODEL

In the present work, direct photon spectra are calculated in the framework of the microscopic Ultrarelativistic Quantum Molecular Dynamics (UrQMD) transport model [27–29], using the hybrid option introduced in ver-

*Electronic address: baeuchle@th.physik.uni-frankfurt.de

EoS	$\epsilon_{\rm crit}$
HG-EoS	$5\epsilon_0$
χ-EoS	$7\epsilon_0$
BM-EoS	$5\epsilon_0$

TABLE I: The critical energy densities for the mapping from hydrodynamics to transport theory for the various Equations of state. $\epsilon_0 = 146$ MeV/fm^3 is the nuclear ground state energy density.

sion 3.3 [30–32, 39]. While UrQMD itself is a hadronic transport model that includes only hadronic and string degrees of freedom and employs PYTHIA [33] for scatterings at high momentum transfer, the hybrid option allows to substitute the high-density part of the evolution by a 3+1-dimensional ideal hydrodynamic [31] description. In this part, other-than-hadronic degrees of freedom and phase transitions may be included.

The inclusion of an intermediate phase into the model raises the need for two interfaces, to go from the particle-based description of the transport model to the density-based description of the hydrodynamic model and back again.

The mapping from transport simulation to hydrodynamics is performed at $t_{\rm start} = 0.6$ fm. Here, the energy-density, baryon number-density and momentum densities are calculated from all particles at midrapidity. Particles with a rapidity $|y| > 2$ are propagated in the cascade and do not interact with the bulk medium.

The transition from hydrodynamics back to the cascade proceeds gradually, mapping the temperatures and chemical potentials to particles via the Cooper-Frye-formula [34] when all cells in the same transverse slice (i.e. at the same position along the beam direction) have diluted below a critical energy density (see Table I). After the transition to the cascade, rescatterings and decays are calculated in the well-known UrQMD model. For more detailed information on the hybrid model the reader is referred to [32, 35].

A. Equations of State

Three different Equations of State (EoS) are compared in this work. The effects of thermalization at the transition from the initial stage cascade to hydrodynamics can be explored with the Hadron Gas-EoS (HG-EoS) [36], which has the same degrees of freedom as the transport phase. To investigate the effects of partonic matter and a phase transition, we use two different models for the EoS: The Chiral Equation of State χ-EoS [37] has a cross-over phase transition to chirally restored and deconfined matter, while the Bag Model Equation of State BM-EoS [31] has a first order phase transition to a Quark Gluon Plasma. In both EoS, the transition happens at around $T_{\rm C} \approx 170$ MeV.

Centrality	$T_{\rm slope}$ [MeV]	A [GeV^{-2}]	χ^2/d.o.f.
00%-10%	231.9± 9.4	2.39±0.67	0.038
00%-92%	231.4± 8.5	0.41±0.11	0.032
10%-20%	234.0±10.0	1.26±0.37	0.041
20%-30%	239.0±11.4	0.56±0.18	0.049
30%-40%	239.0±13.1	0.27±0.10	0.065
40%-50%	243.0±13.4	0.12±0.04	0.064
50%-60%	235.4± 8.8	$(5.64\pm1.43)\cdot10^{-2}$	0.032
60%-92%	250.5±11.8	$(6.91\pm2.08)\cdot10^{-3}$	0.044

TABLE II: Fit results for the low-$p_\perp$-part ($p_\perp < 2.5$ GeV) of the cascade calculations of Au+Au-collisions at $\sqrt{s_{\rm NN}} = 200$ GeV (see Fig. 1). The fit function is $f(p_\perp) = A \exp\left(-\frac{p_\perp}{T_{\rm slope}}\right)$.

B. Photon emission sources

Due to the small creation probability of direct photons, their emission is calculated perturbatively. I.e., the evolution of the underlying event remains unaltered by the emission of direct photons.

The set of channels for direct photon production differ in the transport and hydrodynamic parts of the model. The most important channels, though, are common to both parts, namely $\pi\pi \to \gamma\rho$ and $\pi\rho \to \gamma\pi$. Besides photon emission from the Quark-Gluon-Plasma, channels with strangeness are included in the hydrodynamic part. The corresponding rates for photon emission from each hydrodynamic cell are taken from Turbide *et al.* [15]. In the transport part, additional processes including an η-meson are included. The corresponding cross-sections have been calculated by Kapusta *et al.* [13].

Although Kapusta and Turbide use different Lagrangians to derive their cross-sections and rates, earlier investigations (see [11]) have shown that the thermal rates that can be extracted from Kapusta's cross-sections using this model agree very well with those parametrized by Turbide *et al.*. The same investigations have shown that the contributions of the hadronic processes that are not common to both models contribute about equally, but not significantly to the final spectra. The numerical implementation for direct photon emission is explained in detail in [11].

At high transverse momenta, another source becomes important, namely the prompt contribution from hard scatterings of partons in the initial nuclei. The spectra predicted by NLO-pQCD calculations from Gordon and Vogelsang [38] fit the experimental data from the PHENIX-collaboration [25] rather well at high $p_\perp$. Therefore, the pQCD contributions from [38], scaled by the number of binary collisions $\langle N_{\rm coll}\rangle$ are added to the soft photons calculated here.

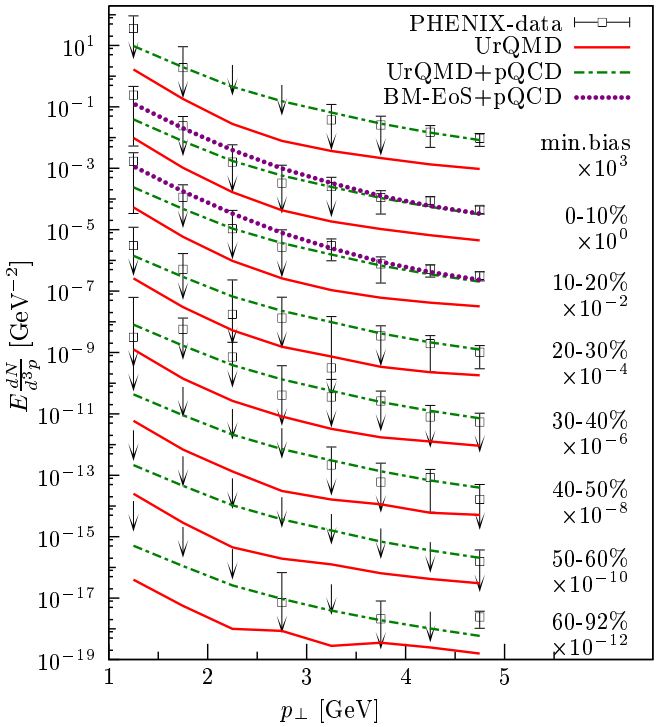

FIG. 1: (Color Online) Comparison of the data from the PHENIX-collaboration [25] (black squares) to cascade calculations (red solid lines) for central to peripheral collisions. The green dash-dotted lines show the sum of pQCD-calculations [25, 38] and the cascade contribution. For the most central collisions, 00-10% and 10-20%, the spectra from hybrid calculations with the BM-EoS plus pQCD-contribution are shown (violett dotted lines).

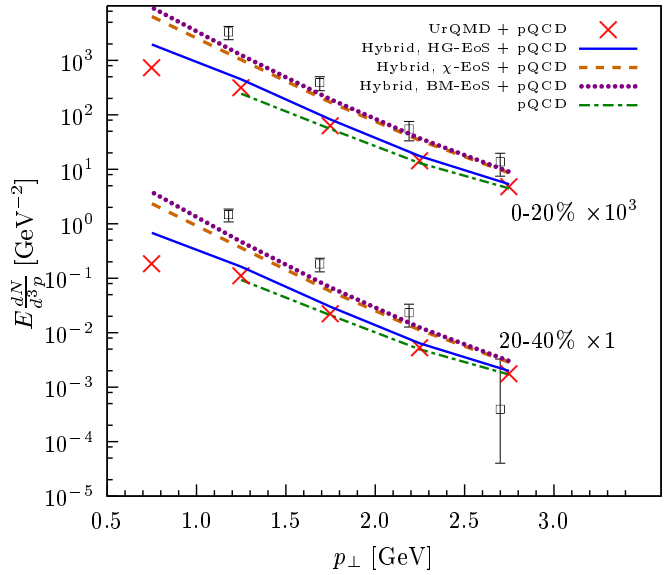

FIG. 2: (Color Online) Comparison of data from the PHENIX-collaboration [26] (black squares) to cascade cacu-lations (red crosses) and hybrid-model calculations with HG-EoS (blue solid lines), χ-EoS (orange dashed lines) and BM-EoS (violett dotted lines) for central (0-20 %) and mid-central (20-40 %) collisions. The contribution from initial pQCD-scatterings [26, 38] have been added to all spectra. The spectra from central collisions have been scaled by a factor of 10^3 to enhance readability.

III. RESULTS

The comparison between direct photon spectra at low and intermediate transverse momentum $p_\perp$ from cascade calculations and data from the PHENIX collaboration [25] for Au+Au-collisions at $\sqrt{s_{\mathsf{NN}}} = 200$ GeV is shown in Fig. 1. One clearly observes that the hadronic transport model (full lines) does not saturate the upper limits of the experimental data. In all centrality bins, the prompt photon yield is significantly larger than predicted by the hadronic cascade. The ratio between pQCD and hadronic contributions is fairly constant among the centrality bins. For comparison, Fig. 1 also shows the spectra obtained with the hybrid model using the Bag Model EoS (BM-EoS) for the two most central bins, 00-10% and 10-20%, which agrees nicely with the data. Thermal fits to the low-$p_\perp$-parts of the cascade spectra show inverse slope parameters of $T_{\mathsf{slope}} \approx 235$ MeV throughout the centrality bins, see Table II.

A more detailed exploration of the low-$p_\perp$-part of the direct photon calculation is shown in Fig. 2. Here, the low-$p_\perp$-data obtained by extrapolating the dilepton yield to zero invariant mass [26] for central (00-20%) and mid-central (20-40%) is shown in comparison to cascade calculations (red crosses) and hybrid calculations with hadron gas EoS (HG-EoS, solid blue lines), chiral EoS (χ-EoS, dashed orange lines) and bag model EoS (BM-EoS, dotted violett lines) and prompt (pQCD) photon calculations. All calculated spectra include the $\langle N_{\mathsf{coll}}\rangle$-scaled prompt photon contribution.

In both centrality-bins, the direct photon spectra obtained with the BM-EoS and χ-EoS, which include a phase transition to a deconfined state of matter, are significantly higher than the hadronic HG-EoS-calculations and agree with the measured data.

A similar picture presents itself in Au+Au-collisions at lower incident energy $\sqrt{s_{\mathsf{NN}}} = 62.4$ GeV and $\sqrt{s_{\mathsf{NN}}} = 130$ GeV, shown in the upper panels of Figure 3. The cascade calulations have been omitted from the Figure for clarity.

Thermal fits to the spectra (see Table III) show inverse slope parameters in the range from $233 < T_{\mathsf{slope}} < 262$ MeV, with the cascade calculations showing the smallest and the χ-EoS hybrid calculations showing the largest values of T_{slope}. HG-EoS and BM-EoS calculations show similar inverse slope parameters. The integrated yield A is highest in BM-EoS hybrid calculations. The spectra from the hybrid calculations are rather similar for the different beam energies.

Hybrid model calculations for central (0-20%) and mid-central (20-40%) Cu+Cu-collisions are shown in the lower panels of Figure 3 for all EoS. The thermal fits (see Ta-

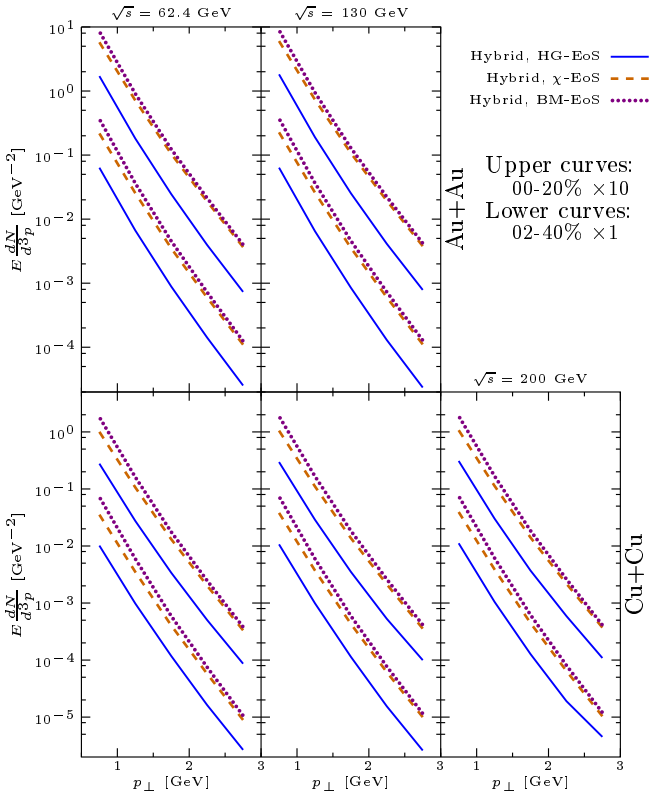

FIG. 3: (Color Online). Direct photon spectra calculated with the Hybrid model and HG-EoS (solid blue lines), χ-EoS (dashed orange lines) and BM-EoS (dotted violett lines) without prompt photon contribution. The left panels show calculations for $\sqrt{s_{\mathsf{NN}}}$ = 62.4 GeV, the middle panels show calculations for $\sqrt{s_{\mathsf{NN}}}$ = 130 GeV and the right panel shows calculations for $\sqrt{s_{\mathsf{NN}}}$ = 200 GeV. The upper panels show calculations for Au+Au-collisions, while the lower panel show calculations for Cu+Cu-collisions. In each panel, the upper curves are central collisions (00-20%) and the lower curves are mid-central collisions (20-40%).

$\sqrt{s_{\mathsf{NN}}}$	EoS	centr.	T_{slope} [MeV]	A [GeV^{-2}]	$\frac{\chi^2}{\text{d.o.f.}}$
200	Transport	0-20%	232.5± 9.8	1.65±0.48	0.041
200	HG-EoS	0-20%	246.7± 8.6	3.63±0.83	0.025
200	χ-EoS	0-20%	261.9± 8.7	10.13±2.05	0.020
200	BM-EoS	0-20%	251.4± 9.7	16.37±4.03	0.029
200	Transport	20-40%	237.3±12.1	0.38±0.13	0.057
200	HG-EoS	20-40%	243.4± 8.3	1.32±0.30	0.025
200	χ-EoS	20-40%	253.0± 8.0	4.11±0.82	0.020
200	BM-EoS	20-40%	240.6± 9.0	7.61±1.90	0.030
130	Transport	0-20%	232.5± 9.1	(9.87±2.67)*	0.035
130	HG-EoS	0-20%	246.3± 8.5	3.42±0.66	0.024
130	χ-EoS	0-20%	261.2± 8.5	9.67±1.93	0.019
130	BM-EoS	0-20%	250.2± 9.6	15.84±3.88	0.039
130	Transport	20-40%	257.2±11.3	(5.48±1.50)$^+$	0.036
130	HG-EoS	20-40%	242.4± 7.6	1.26±0.26	0.021
130	χ-EoS	20-40%	252.7± 7.9	4.01±0.80	0.019
130	BM-EoS	20-40%	240.6± 8.8	7.46±1.82	0.029
62.4	Transport	0-20%	242.1±13.5	(5.29±1.95)*	0.066
62.4	HG-EoS	0-20%	247.3± 8.1	3.19±0.67	0.022
62.4	χ-EoS	0-20%	261.8± 8.2	9.24±1.78	0.018
62.4	BM-EoS	0-20%	250.3± 9.5	15.13±3.65	0.028
62.4	Transport	20-40%	232.8± 9.4	(4.18±1.16)$^+$	0.038
62.4	HG-EoS	20-40%	245.8± 8.0	1.21±0.26	0.022
62.4	χ-EoS	20-40%	253.9± 7.7	3.82±0.73	0.018
62.4	BM-EoS	20-40%	240.8± 8.6	7.33±1.74	0.028

*: $\times 10^{-2}$, $^+$: $\times 10^{-3}$

TABLE III: Fit results for the low-$p_\perp$-part ($p_\perp < 2.5$ GeV) of the spectra from central (0-20%) and mid-central (20-40%) Au+Au-collisions. The fit function is $f(p_\perp) = A \exp\left(-\frac{p_\perp}{T_{\mathsf{slope}}}\right)$. The data are shown in Figure 2 (for $\sqrt{s_{\mathsf{NN}}}$ = 200 GeV) and Figure 3 ($\sqrt{s_{\mathsf{NN}}}$ = 62.4 GeV, upper left panel and $\sqrt{s_{\mathsf{NN}}}$ = 130 GeV, upper central panel).

ble IV) again show no significant energy dependence of inverse slope parameter T_{slope} or yield A. We observe a clear ordering of the total yield between the Equations of State, with yield from the BM-EoS calculations being higher than that of the χ-EoS, and both yields exceeding that of HG-EoS calculations. However, the inverse slope parameters are similar in HG-EoS and χ-EoS calculations but significantly lower in BM-EoS calculations.

IV. SUMMARY

We examined the direct photon spectra obtained with a transport and a transport+hydrodynamics hybrid model for collisions of Au+Au and Cu+Cu at energies of $\sqrt{s_{\mathsf{NN}}}$ = 62.4, 130 and 200 GeV. We find that the hadronic models (transport model and hybrid model with Hadron Gas EoS) underpredict the data, while calculations with a deconfined state of matter (hybrid model with Chiral or Bag Model EoS) fit the data much better.

Thermal fits to the data show no significant beam energy dependence on the spectra. The inverse slope parameters obtained by fitting the low-transverse momentum part of the spectra are in the range of $227 < T_{\mathsf{slope}} < 262$ MeV, which is significantly above the expected transition temperature to deconfined matter.

Prompt photons from the initial early hard proton-proton scatterings are found to be a significant source of direct photon emission above $p_\perp = 3.5$ GeV, if an EoS with phase transition is assumed, and is dominant throughout all $p_\perp$ if a purley hadronic scenario is assumed.

V. OUTLOOK

Future work with this model will include the extraction of radial and elliptic flow parameters v_1 and v_2 for more differential analyses. Also, the influence of chang-

$\sqrt{s_{NN}}$	EoS	centr.	T_{slope} [MeV]	A [GeV^{-2}]	$\frac{\chi^2}{d.o.f.}$
200	HG-EoS	0-20%	252.0± 9.6	$(4.84\pm1.38)^{\times}$	0.057
200	χ-EoS	0-20%	251.5± 7.3	1.77±0.39	0.033
200	BM-EoS	0-20%	237.7± 7.8	3.61±0.94	0.047
200	HG-EoS	20-40%	254.6±13.2	$(1.61\pm0.62)^{\times}$	0.103
200	χ-EoS	20-40%	242.9± 7.0	$(7.25\pm1.63)^{\times}$	0.036
200	BM-EoS	20-40%	229.2± 7.5	1.60±0.43	0.051
130	HG-EoS	0-20%	250.0± 9.3	$(4.78\pm1.35)^{\times}$	0.056
130	χ-EoS	0-20%	250.9± 7.1	1.76±0.37	0.031
130	BM-EoS	0-20%	238.1± 7.9	3.56±0.93	0.048
130	HG-EoS	20-40%	240.4± 7.7	$(1.99\pm0.50)^{\times}$	0.044
130	χ-EoS	20-40%	242.8± 7.1	$(6.99\pm1.59)^{\times}$	0.036
130	BM-EoS	20-40%	228.5± 7.7	1.58±0.44	0.054
62.4	HG-EoS	0-20%	248.2± 7.7	$(4.71\pm1.11)^{\times}$	0.039
62.4	χ-EoS	0-20%	250.2± 6.8	1.71±0.35	0.029
62.4	BM-EoS	0-20%	236.8± 7.4	3.52±0.88	0.044
62.4	HG-EoS	20-40%	242.8± 6.9	$(1.87\pm0.41)^{\times}$	0.034
62.4	χ-EoS	20-40%	241.7± 6.3	$(6.71\pm1.37)^{\times}$	0.029
62.4	BM-EoS	20-40%	227.0± 6.7	1.62±0.40	0.042

$^{\times}$: $\times 10^{-1}$

TABLE IV: Fit results for the low-$p_\perp$-part ($p_\perp < 2.5$ GeV) of the spectra from central (0-20%) and mid-central (20-40%) Cu+Cu-collisions. The fit function is $f(p_\perp) = A \exp\left(-\frac{p_\perp}{T_{\rm slope}}\right)$. The data are shown in Figure 3, lower panels.

ing the criteria for the transition between the transport- and hydrodynamic phases in the hybrid model will be examined in the future.

VI. ACKNOWLEDGEMENTS

This work has been supported by the Frankfurt Center for Scientific Computing (CSC), the GSI and the BMBF. B. Bäuchle gratefully acknowledges support from the Deutsche Telekom Stiftung, the Helmholtz Research School on Quark Matter Studies and the Helmholtz Graduate School for Hadron and Ion Research. This work was supported by the Hessian LOEWE initiative through the Helmholtz International Center for FAIR.

The authors thank Elvira Santini for valuable discussions and Henner Büsching for experimental clarifications.

[1] J. W. Harris and B. Muller, Ann. Rev. Nucl. Part. Sci. **46** (1996) 71 [arXiv:hep-ph/9602235].
[2] S. A. Bass, M. Gyulassy, H. Stoecker and W. Greiner, J. Phys. G **25** (1999) R1 [arXiv:hep-ph/9810281].
[3] S. S. Adler *et al.* [PHENIX Collaboration], Phys. Rev. Lett. **91** (2003) 072301 [arXiv:nucl-ex/0304022].
[4] S. S. Adler *et al.* [PHENIX Collaboration], Phys. Rev. C **69** (2004) 034910 [arXiv:nucl-ex/0308006].
[5] J. Adams *et al.* [STAR Collaboration], Nucl. Phys. A **757** (2005) 102 [arXiv:nucl-ex/0501009].
[6] B. B. Back *et al.*, Nucl. Phys. A **757** (2005) 28 [arXiv:nucl-ex/0410022].
[7] I. Arsene *et al.* [BRAHMS Collaboration], Nucl. Phys. A **757** (2005) 1 [arXiv:nucl-ex/0410020].
[8] K. Adcox *et al.* [PHENIX Collaboration], Nucl. Phys. A **757** (2005) 184 [arXiv:nucl-ex/0410003].
[9] C. Gale, arXiv:0904.2184 [hep-ph].
[10] A. Dumitru, M. Bleicher, S. A. Bass, C. Spieles, L. Neise, H. Stoecker and W. Greiner, Phys. Rev. C **57** (1998) 3271 [arXiv:hep-ph/9709487].
[11] B. Bauchle and M. Bleicher, Phys. Rev. C **81** (2010) 044904 [arXiv:0905.4678 [hep-ph]].
[12] E. L. Bratkovskaya, S. M. Kiselev and G. B. Sharkov, Phys. Rev. C **78** (2008) 034905 [arXiv:0806.3465 [nucl-th]].
[13] J. I. Kapusta, P. Lichard and D. Seibert, Phys. Rev. D **44** (1991) 2774 [Erratum-ibid. D **47** (1993) 4171].
[14] D. K. Srivastava and B. Sinha, Phys. Rev. C **64** (2001) 034902 [arXiv:nucl-th/0006018].
[15] S. Turbide, R. Rapp and C. Gale, Phys. Rev. C **69** (2004) 014903 [arXiv:hep-ph/0308085].
[16] S. Turbide, C. Gale, S. Jeon and G. D. Moore, Phys. Rev. C **72** (2005) 014906 [arXiv:hep-ph/0502248].
[17] F. M. Liu, T. Hirano, K. Werner and Y. Zhu, J. Phys. G **36** (2009) 064072 [arXiv:0811.0666 [hep-ph]].
[18] F. M. Liu, T. Hirano, K. Werner and Y. Zhu, Phys. Rev. C **80** (2009) 034905 [arXiv:0902.1303 [hep-ph]].
[19] K. Dusling, Nucl. Phys. A **839** (2010) 70 [arXiv:0903.1764 [nucl-th]].
[20] K. Dusling and I. Zahed, arXiv:0911.2426 [nucl-th].
[21] M. M. Aggarwal *et al.* [WA98 Collaboration], arXiv:nucl-ex/0006007.
[22] M. M. Aggarwal *et al.* [WA98 Collaboration], Phys. Rev. Lett. **85** (2000) 3595 [arXiv:nucl-ex/0006008].
[23] M. M. Aggarwal *et al.* [WA98 Collaboration], Phys. Rev. Lett. **93** (2004) 022301 [arXiv:nucl-ex/0310022].
[24] A. Adare *et al.* [PHENIX Collaboration], Phys. Rev. C **81** (2010) 034911 [arXiv:0912.0244 [nucl-ex]].
[25] S. S. Adler *et al.* [PHENIX Collaboration], Phys. Rev. Lett. **94** (2005) 232301 [arXiv:nucl-ex/0503003].
[26] A. Adare *et al.* [PHENIX Collaboration], Phys. Rev. Lett. **104** (2010) 132301 [arXiv:0804.4168 [nucl-ex]].
[27] S. A. Bass *et al.*, Prog. Part. Nucl. Phys. **41** (1998) 255 [Prog. Part. Nucl. Phys. **41** (1998) 225] [arXiv:nucl-th/9803035].
[28] M. Bleicher *et al.*, J. Phys. G **25** (1999) 1859 [arXiv:hep-

ph/9909407].
[29] H. Petersen, M. Bleicher, S. A. Bass and H. Stocker, arXiv:0805.0567 [hep-ph].
[30] D. H. Rischke, S. Bernard and J. A. Maruhn, Nucl. Phys. A **595** (1995) 346 [arXiv:nucl-th/9504018].
[31] D. H. Rischke, Y. Pursun and J. A. Maruhn, Nucl. Phys. A **595** (1995) 383 [Erratum-ibid. A **596** (1996) 717] [arXiv:nucl-th/9504021].
[32] H. Petersen, J. Steinheimer, G. Burau, M. Bleicher and H. Stocker, Phys. Rev. C **78** (2008) 044901 [arXiv:0806.1695 [nucl-th]].
[33] T. Sjostrand, S. Mrenna and P. Z. Skands, JHEP **0605** (2006) 026 [arXiv:hep-ph/0603175].
[34] F. Cooper and G. Frye, Phys. Rev. D **10** (1974) 186.
[35] J. Steinheimer, V. Dexheimer, H. Petersen, M. Bleicher, S. Schramm and H. Stoecker, [arXiv:0905.3099 [hep-ph]].
[36] D. Zschiesche, S. Schramm, J. Schaffner-Bielich, H. Stoecker and W. Greiner, Phys. Lett. B **547** (2002) 7 [arXiv:nucl-th/0209022].
[37] J. Steinheimer, S. Schramm and H. Stocker, arXiv:0909.4421 [hep-ph].
[38] L. E. Gordon and W. Vogelsang, Phys. Rev. D **48** (1993) 3136.
[39] UrQMD v3.3 is available at http://urqmd.org/